Building and Environment 137 (2018) 246–256

Contents lists available at ScienceDirect

Building and Environment

journal homepage: www.elsevier.com/locate/buildenv

Field measurement of natural ventilation rate in an idealised full-scale building located in a staggered urban array: Comparison between tracer gas and pressure-based methods

H.L. Gough[a,*], Z. Luo[b], C.H. Halios[a], M.-F. King[c], C.J. Noakes[c], C.S.B. Grimmond[a], J.F. Barlow[a], R. Hoxey[d], A.D. Quinn[d]

[a] Department of Meteorology, University of Reading, United Kingdom
[b] School of the Built Environment, University of Reading, United Kingdom
[c] School of Civil Engineering, University of Leeds, United Kingdom
[d] School of Civil Engineering, University of Birmingham, B15 2TT, United Kingdom

ARTICLE INFO

Keywords:
Natural ventilation
Ventilation rate
Tracer gas
Full-scale
Pressure
Wind direction

ABSTRACT

Currently, no clear standards exist for determining urban building natural ventilation rates, especially under varying realistic meteorological conditions. In this study, ventilation rates are determined using tracer gas decay and pressure-based measurements for a full-scale (6 m tall) cube. The cube was either isolated (2 months of observations) or sheltered within a staggered array (7 months), for both single-sided and cross ventilation (openings 0.4 m × 1 m). Wind speeds at cube height ranged between 0.04 m s^{-1} and 13.1 m s^{-1}. Errors for both ventilation methods are carefully assessed. There is no discernible linear relation between normalised ventilation rates from the two methods, except for cross ventilation in the array case. The ratio of tracer gas and pressure derived ventilation rates is assessed with wind direction. For single-sided (leeward opening) cases it approached 1. For cross ventilation the ratio was closer to 1 but with more scatter. One explanation is that agreement is better when internal mixing is less jet-dominated, i.e. for oblique directions in the isolated case and for all directions for unsteady array flows. Sheltering may reduce the flushing rate of the tracer gas from the cube relative to internal mixing rate. This new dataset provides an extensive range of conditions for numerical model evaluation and for understanding uncertainty of ventilation rates. Knowledge of the latter is critical in building design.

1. Introduction

Accurate predictions of ventilation rates are required for the health and well-being of the occupants inside a building. Natural ventilation is suited to mild climates [47] to create a comfortable and healthy indoor environment, and save energy compared to mechanical ventilation systems [11,26]. A variety of tools are used to simulate natural ventilation: EnergyPlus (e.g. [54]), TRNSYS coupled with CONTAM (e.g. [31]) and CFD (Computer Fluid Dynamics) models (e.g. [32,33,69]). To verify natural ventilation simulations, detailed datasets are required with temperature, internal gains, operable window position, tracer gas concentrations and air velocity observed [42]. Given natural ventilation's dependence on the external conditions, many studies use test chambers (e.g. [58,69]) or wind tunnel models (e.g. [35]) to control the boundary conditions, but lose the true information of the impact from varying atmospheric conditions. Full-scale measurements in true atmospheric conditions are limited, because of the variability of external conditions, measurement difficulties and cost limitations [42]. Furthermore, determining natural ventilation rate in the urban environment is more challenging due to the complex wind environment and all scales of turbulence encountered [1].

To date few full-scale studies of natural ventilation within an urban area have been undertaken, though most agree that natural ventilation becomes less effective in urban areas [13,14,63]. For isolated buildings, opening shape, size and location [45,56,65] could affect natural ventilation performance. Instantaneous fluctuations in wind direction and wind speed also have an effect [24]. To our best knowledge, the long-term measurement of natural ventilation for both isolated and array cases under the varying realistic atmospheric conditions, allowing the direct comparison of the two, has never been studied.

In terms of methods for full-scale measurement of natural ventilation rate, both tracer gas techniques and pressure taps are the most

* Corresponding author. Department of Meteorology, University of Reading, Earley Gate, PO Box 243, Reading, RG6 6BB, United Kingdom.
E-mail address: h.gough@reading.ac.uk (H.L. Gough).

https://doi.org/10.1016/j.buildenv.2018.03.055
Received 22 January 2018; Received in revised form 15 March 2018; Accepted 28 March 2018
Available online 29 March 2018

frequently used [9,46]. Despite the study of ventilation becoming more multi-disciplinary, there is no clear guidance on which method to use and how methods compare for realistic buildings in actual meteorological conditions. Typically, average climate data are used, which by definition, missing both the extremes and the variability.

Comparisons between pressure difference and tracer gas methods for naturally ventilated livestock buildings [10,52] found pressure difference methods were unable to provide 'accurate' estimates or of true ventilation rate because of the dependence on wind speed. Unfortunately, the inaccuracy was not quantified.

The objective of this paper is to compare tracer gas and pressure-based methods to determine ventilation rates in a full-scale field environment (both isolated and building array), with a detailed methodology and error analysis. The mean ventilation rates are determined with tracer gas decay (Section 2.1) and pressure-based (Section 2.2) methods for a ventilated 6 m high cube in an isolated and staggered cube array and with cross and single-sided ventilation. Mean ventilation rates are compared over a range of weather conditions and wind directions.

2. Description of tracer gas and pressure-based methods

2.1. Tracer gas decay method

Determining ventilation rates through measurement of tracer gas concentrations is best suited to single zone systems or where sections of a building can be completely isolated [55]. The tracer gas methods commonly used are constant injection (e.g. [66]), constant concentration (e.g. [4]) and tracer gas decay (e.g. [9]). Of the three, the decay method is more common, as smaller amounts of gas are required and it is easier to implement [44].

Despite carbon dioxide (CO_2) being naturally present in the atmosphere, it is commonly used as an indoor air quality indicator and as a tracer gas. Advantages includes its low cost and straightforward safety requirements. CO_2 can be released (e.g. [9,16]) or generated by room occupants (e.g. [39,70]) to be utilised [41]. Other gases used include sulphur hexafluoride (SF_6) [57], sulphur dioxide (SO_2) [18], carbon monoxide (CO) [59,67] and nitrogen dioxide (NO_2) [68].

Few guidelines for sensor positioning are available [21] [22]; despite this being crucial to obtaining representative measurements [40]. Within mechanically ventilated rooms, inappropriate sensor positioning can cause tracer gas decay ventilation rate errors of up to 85% [62]. Van Buggenhout et al. recommend siting at the ventilation outlet, while acknowledging wind speed, thermal effects and wind direction may make this impractical. This lack of guidance combined with other experimental aspects can make comparison of results difficult [40]. Basic comparisons require: measurement method, application details, instrumentation and their calibrations, timings, number of measurements, meteorological conditions and building conditions [48]. found only half of [60] 26 studies gave instrumentation details and only 4 of the 26 provided measurement uncertainty values.

Tracer gas ventilation rates stem from the mass-balance equation [36]:

$$V\frac{dC_i(t)}{dt} = (C_a - C_i(t))Q + E \quad (1)$$

where V (m^3) is the room volume, Q ($m^3\ s^{-1}$) is the volumetric flow rate, C_i ($kg\ m^{-3}$) is the indoor concentration of tracer gas, C_a ($kg\ m^{-3}$) is the external concentration of tracer gas, E ($kg\ s^{-1}$) is the amount of tracer gas emitted from an indoor source and t *(s)* is time. C_iQ is the transport of tracer gas from the room to the outside through openings or cracks and C_aQ is the transport of tracer gas from the outside into the room. If no indoor source is present, then by integrating equation (1) the indoor concentration is:

$$C_i(t) = (C_0 - C_a)\exp(-\lambda t) + C_a \quad (2)$$

where C_0 is the concentration of gas when $t = 0$ and λ is the ventilation rate in air changes per hour (h^{-1}). To derive ventilation rate, taking the natural logarithm of equation (2) gives a linear relation with slope λ:

$$\ln(C_i(t) - C_a) = \ln(C_0 - C_a) - \lambda t \quad (3)$$

Ventilation rates (Q, in $m^3\ s^{-1}$) can be converted to λ (h^{-1}) using:

$$\lambda = \frac{3600\ Q}{V} \quad (4)$$

Here all ventilation rates are in $m^3\ s^{-1}$ unless otherwise stated. Equation (3) requires several assumptions [36,55]:

- The tracer gas is chemically inert, with the room objects neither absorbing nor releasing the tracer gas;
- Room air is well-mixed; i.e., C_i is spatially uniform;
- Exchange of internal and external air occurs in places with direct contact with the outside; e.g. windows;
- Room is a single zone system.

Differences in room temperature may lead to stratification, ineffective mixing and the presence of dead-zones within a room [62].

2.2. Pressure-based method

Pressure differences across a building provide a second ventilation rate method. Either the internal-external or windward - leeward external face (e.g. [12,25,59]) pressure differences may be used. An alternative to direct pressure measurement is to assume a pressure coefficient can be estimated. However, the effects of urban surroundings on pressure coefficients (e.g. [2,32,33,64]); are not well known. Research to determine pressure coefficients often focuses on parts of a building design, e.g. wind towers [28]. The review by [8] of pressure coefficient data models highlighted that significant variations in estimates occur between sources. Given the lack of pressure coefficient data for low wind speeds ($< 4\ m\ s^{-1}$), building ventilation rates for these conditions are rare. The relative role of thermal or wind driven processes poorly understood [8].

If a pressure difference (Δp) between the internal and external environments or between the front and back of a building can be deduced, the flow rate through the opening (Q_p) is:

$$Q_p = C_d A\sqrt{\frac{2\,\Delta p}{\rho}} \quad (5)$$

where ρ is the air density. C_dA is the effective area of an opening. This changes with the number of openings and their relative positions. C_d is the discharge coefficient and A is the opening area. The assumptions required for equation (5) are:

- flow is turbulent under normal pressures,
- kinetic energy is dissipated at the windward opening
- presence of openings does not influence the surface pressure distribution.

For cross ventilation with both inlets and outlets, some of the turbulent kinetic energy can be preserved and directed outside without interior dissipation, undermining the kinetic energy assumption [30,43]. Suggested alternatives (e.g. [23,30,53]) have not replaced the orifice equation.

The largest source of error arises from using a mean rather than instantaneous pressure differences [6]. Uncertainty increases with very large (undefined) openings [46] as non-uniform pressure differences occur and the ventilation opening velocity profiles vary with time. Errors arise if an incorrect discharge coefficient is used, as C_d is sensitive to opening size and wind direction and also for cross ventilation, the ratio of the two openings [5,29].

Table 1
Equipment used for measurements of data analysed.

Variable	Manufacturer Model Instrument Sampling Frequency	Specifications
Velocity Direction	Gill Windmaster R3-50 Sonic Anemometer 10 Hz (20 Hz on Channel mast) [15]	Velocity: Range: 0–45 m s^{-1} Resolution: 0.01 m s^{-1} Accuracy: < 1.5% RMS at 12 m s^{-1} Direction: Range: 0–359° Resolution: 0.1° Accuracy: 2° at 12 m s^{-1}
External CO_2	LI-COR LI-7500 Infra-red gas analyser 20 Hz (LI-COR [38]	Range CO2: 0–3000 ppm Accuracy CO2: 1% of reading
Internal CO_2	Senseair K30 FR 2 Hz 1% non-dispersive infra-red (NDIR) CO2 Sensor 2 Hz [7]	Range: 0–10000 ppm Error: ± 20 ppm ± 1% of measured value Accuracy: ± 30 ppm ± 3% of measured value Response time: 2 s at 0.5 L min^{-1} flow 20 s diffusion time
Surface pressure	Honeywell Analogue Pressure taps 10 Hz [20]	1:16 Range: −2.5 to 2.5 Inches of H2O Honeywell 163PC01D75 17:32 Range: 5 to 5 Inches of H2O Honeywell 163PC01D76 Response time (all): 1 ms Drift (all) 0.5% of measurement span per year
Internal temperature	RS components Type-K Thermocouples (0.2 mm diameter) 10 Hz [51]	Range: −100 to 250 °C Error: ± 1.5 °C ± 0.25% Response time in moving air: 0.1 s Diameter: 0.2 mm
Velocity, External temperature Surface pressure, Humidity Precipitation	Vaisala WXT520 Weather Station 20 Hz [61]	Wind Speed Accuracy: ± 3% at 10 m s^{-1} Wind direction Accuracy: ± 3° Wind Response time: 250 ms Air temperature accuracy at 20 °C: ± 0.3 °C Humidity 0–90% accuracy: ± 3% Pressure accuracy at 0–30 °C: ± 5 hPa Precipitation accuracy: ± 5%
Shortwave and longwave radiation	Kipp and Zonen CNR4 20 Hz [34]	Response time: < 18 s Non-Linearity: < 1% Sensitivity: 5 to 20 μ V/W/m^2

3. Experimental design

Observations were undertaken within the REFRESH (Remodelling Building Design Sustainability from a Human Centred Approach) Cube Campaign (RCC). Full details of the array set-up, external and internal flow patterns and an overview of the data gathered within RCC-REFRESH are given in [16,17,32,33]. Details pertaining to the determination of ventilation rates are given here.

Observations (Table 1) were taken at Wrest Park, Silsoe, Bedfordshire, U.K. (52.01088° N, −0.410979° W) using an uninhabited instrumented cube (height 6 m). The cube, was clad in flat, steel sheets to ensure uniform external surfaces. It was positioned to be perpendicular to the prevailing site wind direction (Fig. 1). Observations occurred in two phases, with the instrumented cube: (i) surrounded by a limited staggered array of eight cubes (October 2014–April 2015) and (ii) isolated (May–July 2015). Therefore, radiative differences occur between the array (winter – spring) and isolated (early summer) cases. These are accounted for as far as possible within the analysis. The real-world environmental factors are used to characterise the measurements.

The cube's front and back faces had removable panels (0.4 m wide x 1 m high) allowing both a sealed and a ventilated structure. Both single-sided and cross ventilated set-ups were used with the centre point of the opening 3.5 m above from the ground (Fig. 1a). This is smaller than the 1 m^2 openings used by [59] as they found the ventilation rates were too large (gas flushed < 30 s) to accurately measure the tracer gas decay curves and meteorological conditions.

3.1. Temperature measurements

Temperature measurements inside the cube (Table 1) allowed determination of thermal stratification, and with the external temperatures on the Channel mast (Fig. 1, Table 1) the thermally-driven ventilation component. The Vaisala WXT520 weather station was positioned to minimise solar gains. Internal temperatures measured at 24 points (Fig. 2, Table 2) were sampled at 10 Hz to allow the average over a large number of samples in the 30 min value and a reasonably accurate mean.

Eight thermocouples (H1 to H8) were horizontally strung between the windows at a height of 3 m (Table 2b). The other 16 were in four vertical profiles of four thermocouples (T1 to T4), put at varying heights (Table 2a) below 4 m given access limitations. The thermocouple errors (0.45% ± 2 °C, junction error plus thermocouple error) are unsuitable for measuring instantaneous fluctuations in temperature [27]. All thermocouples and the WXT520 were calibrated and corrected (on average < 0.5 °C) for instrument bias at the start and end of the experiment using an environmental chamber (Design Environmental Delta 190H) over a −20 °C to 50 °C range, accounting for hysteresis effects due to instrumental time response.

3.2. Tracer gas decay method set-up

The combination of site limitations, safety concerns, affordability, lower environmental impact, wide range of sensors and lower risks (cf. other tracer gases, e.g. Argon and SF_6) led to CO_2 being chosen as the tracer gas. The external CO_2 concentration (C_a) was measured with an open path LI-COR LI-7500 on the channel mast (Fig. 1, Table 1). During the 10-month study, C_a varied between 365 and 450 ppm (95% between 371 and 403 ppm). Given the low natural variability (standard deviation typically 3–4 ppm) of C_a during a decay experiment (Table 3), the mean C_a for that period is used in equation (3). The LI-COR LI-7500 was sufficiently distant from the cube to ensure the tracer CO_2 releases did not have an effect.

The three synchronised K30 NDIR sensors measuring internal CO_2 (C_i) (Fig. 3, Table 1) were not electronically shielded. They were encased within modified junction boxes to protect from frost, condensation and to reduce magnetic noise (Fig. 3). Pre-experiment checks ensured there was adequate airflow to the sensors.

The K30 sensors were calibrated by the manufacturer and compared in-house to the LI-7500 in both a constant concentration test, and a decay from the sensor upper limit (10,000 ppm) before and after the field campaign. None of the three sensors drifted over the course of the experiment. Fig. 3 shows the 'East' sensor (E) positioned under the east opening (1 m from the wall, 2.75 m above the ground). The 'Low' sensor (L) was hung under the steel girder of the east wall, (1 m from the North-East corner of the cube, 0.3 m above the ground). The 'Middle' sensor (M) was 3 m above the ground at the centre-point of the Northern wall (~0.5 m from the wall) but near a crack between the floor and building to help understand infiltration effects on the ventilation rate. To reduce the infiltration rates, cracks at the cube base were filled with foam. Ideally more sensors would have been used to give more representative results of the cube over-all ventilation rate.

The cube's nine inlet pipes (Fig. 3) were used to release the tracer evenly throughout the cube. A large desk fan (estimated effective range

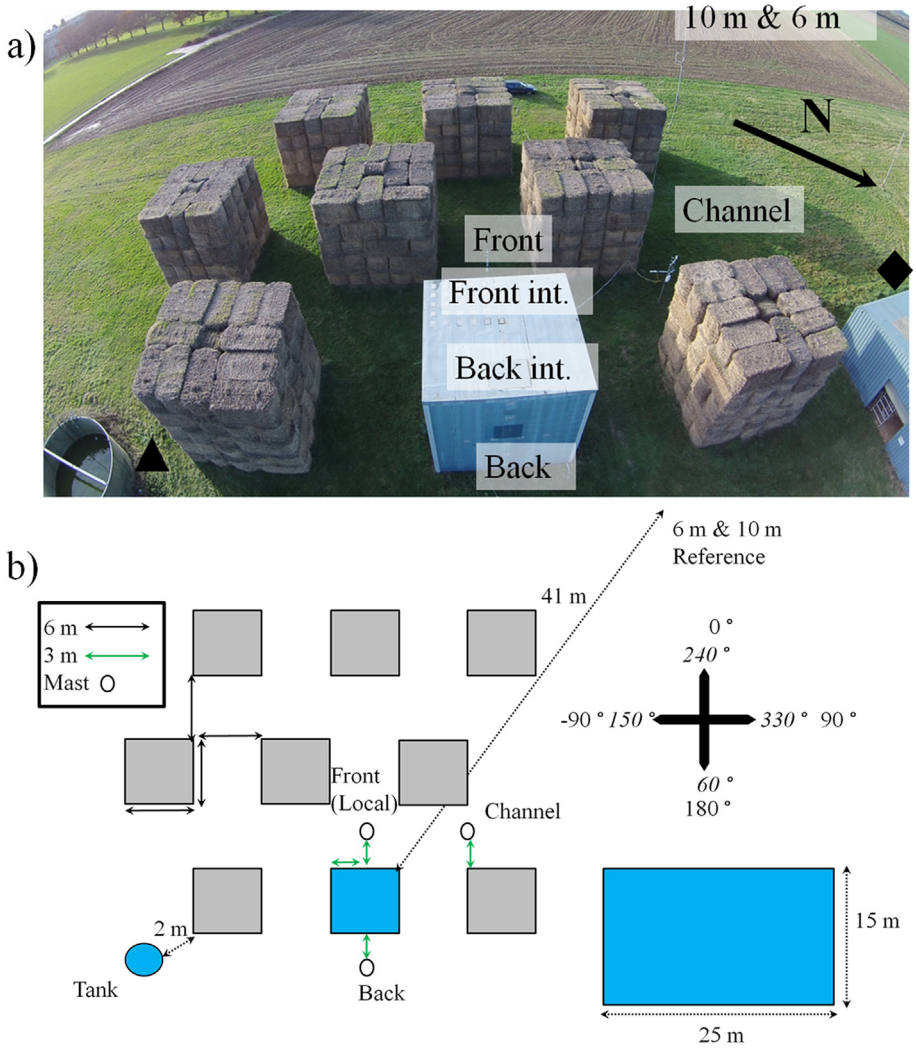

Fig. 1. Cube array and instrument (sonic anemometer, Table 1), storage shed (black diamond) and sewage tanks (black triangle) locations: a) aerial image towards the prevailing wind direction b) plan of the array case with measurements and angle notation. For the isolated case, the grey cubes were removed [17].

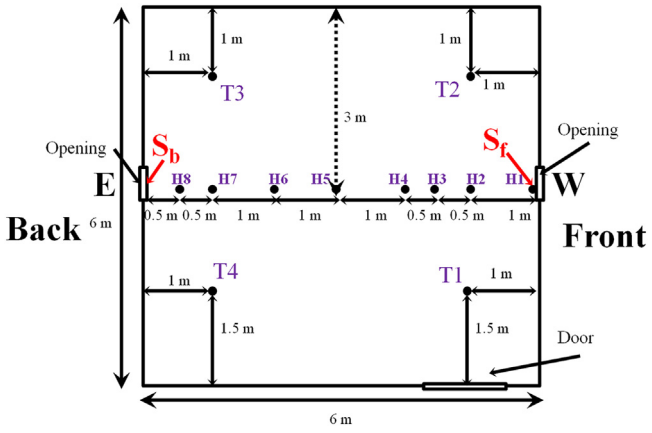

Fig. 2. Locations of the 24 thermocouples (vertical (T1-T4) and horizontal (H) arrays, see Table 2 for heights) and two sonic anemometers (S_f and S_b) within the cube and its openings and door shown.

Table 2
(a) Heights (m) of the thermocouples (T1-T4) and (b) distance (m) from the front internal sonic anemometer (S_f) of the horizontal thermocouples (H) located as shown in Fig. 2.

(a) Number in vertical	Height (m)			
	T1	T2	T3	T4
1	1.0	1.5	3.0	2.0
2	1.5	2.75	2.5	2.5
3	2.5	3.5	1.0	3.5
4	3.0	4.0	0.75	4.0

b)	H8	H7	H6	H5	H4	H3	H2	H1
Distance from S_f (m)	5.5	5.0	4.0	3.0	2.0	1.5	1.0	0.0

of 4 m horizontally, 2 m vertically) was used to improve mixing. Eight outlets were 3 m above floor level. Outlet number 6 was placed at floor level in the centre of the room and had a pipe length (outlet to regulator) of 2.2 m, whereas all others were 3.1 m. The CO_2 was heated by the regulator to approximately 10 °C to prevent the outlet freezing during release and to reduce the temperature difference between the tracer gas and the ambient air. Gas release was controlled externally.

The procedural order for each tracer gas decay experiment was:

1) The openings (if used) were blocked from the outside with a temporary panel. The fan was turned on
2) Sensors were checked for any signs of water damage or loose connections before logging initiated
3) The door was shut, and CO_2 released for 10–15 min. The maximum

Table 3
Number (#) of tracer gas release (Q_t) experiments, mean length of the decay (min) and number of 30 min average pressure (Q_p) measurements for the different ventilation cases when cube was isolated and within the array. Only days with all input data required for calculation are included.

Ventilation case	Isolated			Array		
	Q_t #	Mean length (min)	Q_p #	Q_t #	Mean length (min)	Q_p #
Infiltration	15	201	N/A	9	475	N/A
Single-sided	26	36	763	15	47	907
Cross ventilated	26	16	648	18	24	637

concentration achieved for all runs was between 3000 and 10000 ppm
4) After 10–15 min, the blocking panels were removed, and the gas switched off (fan remained on to aid mixing)
5) The cube was left undisturbed for at least 20 min. For infiltration experiments, the cube was often left over-night due to the low air exchange rate

The local air change rate (λ) for each sensor is calculated by linear fit (equation (3)) incorporating errors (e.g. Fig. 5, section 4.1). The instrumental errors are accounted for in λ by fitting curves to measured data plus and minus the instrumental error (Table 1). The final ventilation rate λ for an experiment is the average of all three sensors when a "well-mixed" criterion is satisfied: (i) flow structure verified by filming smoke release inside the cube or (ii) all 30 min horizontal (difference of the average temperature of H1, H2 and H7, H8) and vertical temperature differences (difference in average temperature of thermocouples at 3–4 m and those at 0–1.5 m) were less than 2.5 °C. The combination of temperature measurements and smoke releases eliminated 15 tracer gas releases from the dataset. Incomplete temperature or smoke data resulted in another 13 being excluded. Thus, 28 out of 156 releases were discarded.

Only the tracer gas method permits infiltration rate measurements, as the area of cracks and gaps could not be determined by other means. The mean infiltration rate (average of 15 infiltration experiments, all wind directions) is 0.562 h^{-1} (0.034 $m^3 s^{-1}$) (median 0.572 h^{-1}) with an inter-quartile range of 0.426 h^{-1} (0.026 $m^3 s^{-1}$) and an error of approximately 5% was removed from the total measured ventilation rate in all results presented (see Table 3).

3.3. Pressure difference

To measure the cube surface pressure, 30 external and 2 internal pressure taps were used. The external pressure taps had 7 mm holes located centrally on 0.6 m^2 steel panels. These were mounted flush to the cube cladding. The taps, located closer together where sharper gradients in pressure were expected (Fig. 4), are in identical positions to [59]. Pressure signals were transmitted pneumatically, using 6 mm internal diameter plastic tubes to transducers located within the cube, at a rate equivalent to 10 Hz. The sensors for taps 1–16 were Honeywell 163PC01D75 differential pressure sensors; pressure taps 17–32 were Honeywell 163PC01D76 differential pressure sensors (Table 1). Two internal pressure taps were located directly under the openings on both the front and back of the cube.

To combat instrument drift, the pressure tap system logged continuously (new file every 30 min). At the start and end of each

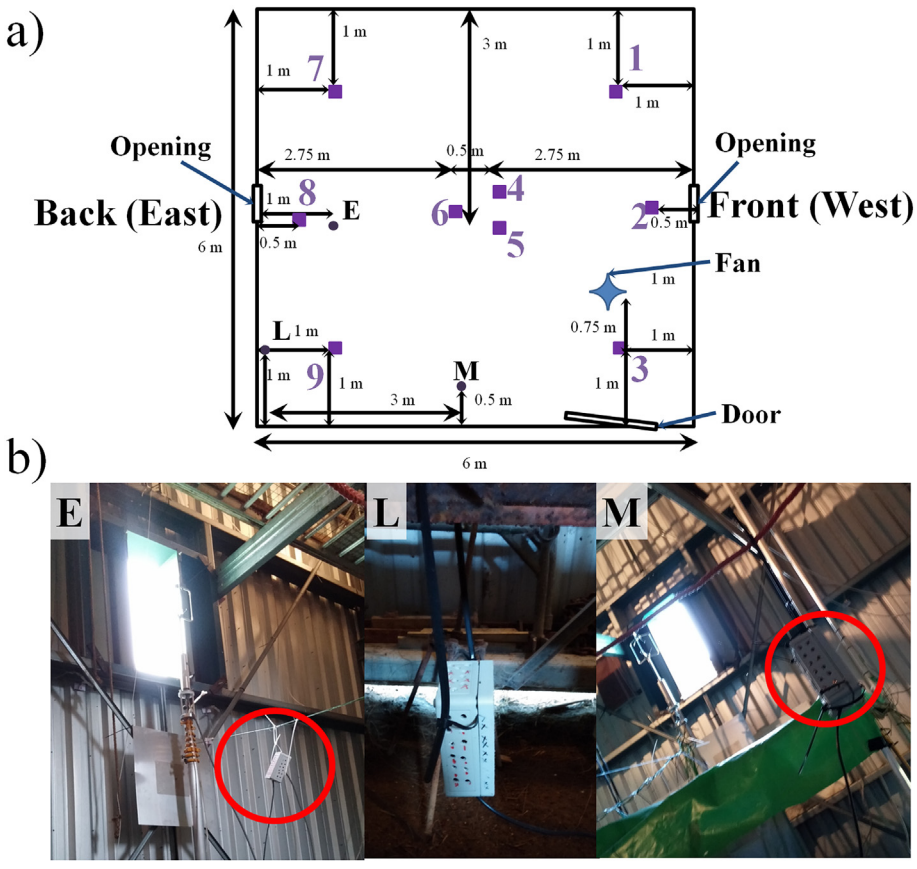

Fig. 3. Tracer gas set-up showing locations of: a) tracer gas inlet pipes (purple squares, 1–9; 1–5 and 7–9 at 3 m above floor level, #6 at ground level), K30 CO_2 sensors (E/L/M, position within 0.1 m), openings (door shown open but closes flush with the wall) and mixing fan (blue cross). b) Photos showing K30 sensors (red circles): Low sensor (L), East sensor (E) and Middle sensor (M). (For interpretation of the references to colour in this figure legend, the reader is referred to the Web version of this article.)

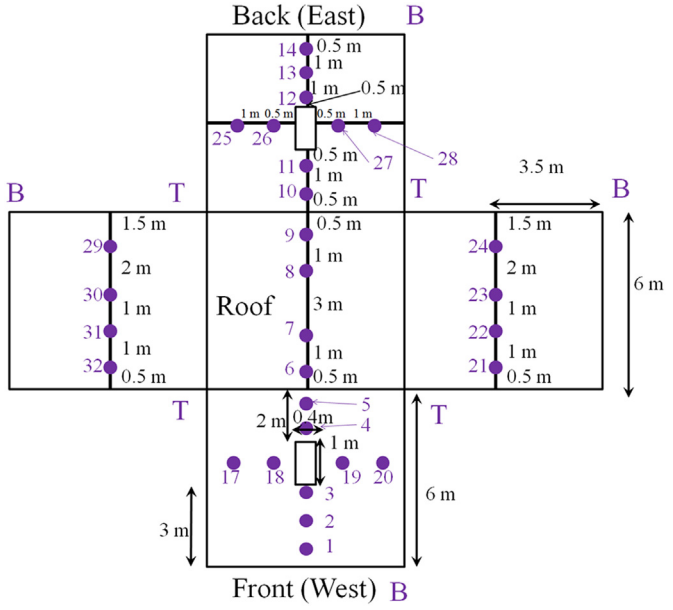

Fig. 4. Location of the pressure taps on each face (T top, B base) of the cube with distance between taps (black) and the opening (white rectangles). Internal taps 15 and 16 are not shown. (drawing not to scale). Front and back faces are symmetrical as are the side faces [17].

measurement file 60 s of zero measurements based on a reference pressure and 60 s of calibration of the pressure transducers to the zero measurements were taken. The last second of data in each file is not analysed as the valves switched to the reference rather than surface pressure.

Reference pressure was measured with a static pressure probe at ground level (custom-built as described in [49]). A reference dynamic pressure was measured using a directional pitot tube [37] at 6 m alongside the 6 m reference sonic anemometer (Fig. 1). External pressure was defined as the mean pressure measured around the opening at the front (Taps 3, 4, 18 and 19) and back (Taps 12, 13, 26 and 27) faces (Fig. 4). Tests undertaken of sealed and ventilated conditions found no effects of the opening on the mean surface pressure measurements closest to the opening.

After the mean of the external taps is calculated, difference calculations (external and internal) are performed for each 10 Hz reading. These differences (averaged per 30 min) is used in equation (5) to calculate Q_P with a flow direction dependent C_d determined from wind tunnel tests. An open-ended wind tunnel (cross section 1.7 m × 1 m, turbulence intensity ~4%) was used with a model of the openings (0.4 m w x 1 m h x 0.23 m d). The sill pointed inwards for the inlet set up and outwards for the outlet set up. A fan within the rig drew air through the inlet cones. This was calibrated to give flow rates from pressure at the conical outlet. Pressures inside the settling chamber box at the downstream end were measured by micro-manometer [50]. The test opening was mounted at the end of the settling box. Temperature, humidity and barometric pressure measurements allow for an accurate calculation of air density. Flow rates and resultant normalised pressure differences were compared, with the gradient between the two being equal to C_dA (Hoxey and Robertson, personal communication, 2015). When acting as an inlet, $C_d = 0.616 \pm 0.016$ and as an outlet, $C_d = 0.658 \pm 0.022$, with errors on C_d being determined from the standard error of the fitted coefficients. The local mean wind direction (Front mast, Fig. 1) is used to select the C_d. If the wind is from $-90°$ to 90° the inlet value is used, otherwise (91° to $-91°$) the outlet value is used. Directional fluctuations (« 30-min) will introduce additional errors into the calculations. The errors in Q_P are calculated with the error propagation method using the standard error of Δp.

Alternatively, the ventilation rates can be calculated for each instantaneous pressure measurement. The average of these is the mean ventilation rate. The two pressure-based methods have approximately a 10% difference in 30-min averages. This decreases to 3–5% for 5-min averages.

3.4. Ventilation measurement summary

Table 3 summarises the ventilation data. The 30 min averaging period for the pressure based ventilation and meteorological variables allows error statistics to be consistent with other meteorological studies [3]. The tracer gas decay length varied with experimental set up. Pressure-based ventilation rates from the full range of observed wind speeds are analysed, unlike earlier pressure coefficient studies which restricted wind speeds (e.g. [19] > 4 m s^{-1} [49], > 3 m s^{-1}). Inclusion of lower wind speeds leads to higher scatter in the range of ventilation rates.

The Archimedes number (*Ar*): ratio of external forces to internal viscous forces can be used to determine whether a flow is being driven by buoyant processes (large *Ar*) or is being affected by external processes (e.g. wind driven, small *Ar*). The dataset has less than 10 cases where buoyant forces are completely dominant; i.e. the most cares are wind driven.

4. Results and discussion

The pressure-based and tracer gas decay results are analysed in three ways: (i) error analysis is discussed and then a single tracer gas release case (< 30 min) is compared to the 1, 5, 10 and 30 min averages for pressure-based ventilation rate (Q_P) for the same period; (ii) the tracer gas decay timestamps are used for the Q_P calculation times; and (iii) all Q_t rates are compared to the 30 min Q_P averages for the entire dataset. The array and isolated cube data are treated separately. For more details about the sheltering effect of the array on the ventilation rate see [17].

To enable comparison across different wind speeds, a normalised ventilation rate (Q_N) is used:

$$Q_N = \frac{Q}{A\ U_{ref}} \tag{6}$$

where U_{ref} is the reference wind speed taken at 6 m (Fig. 1). Tracer gas decay air changes per hour (λ) are converted into Q (m^3 s^{-1}) before being normalised using equation (6).

Pressure difference derived ventilation rates are only used when the data series for that period is complete.

4.1. Case study: isolated cube, cross ventilation

During the isolated cube cross-ventilated case study (21/05/2015) the mean reference wind speed (U_{ref}) is 5.3 m s^{-1} (standard deviation $\sigma_{Uref} = 0.24$ m s^{-1}) and wind direction (θ_{ref}) is 6° ($\sigma_{\theta ref} = 19°$). The total time when the tracer gas was well-mixed within the cube was 9 min. The decay curves (Fig. 5) are only for the 9 min well-mixed data. There is a gap in the pressure difference ventilation rate data (Fig. 6) linked to the system calibration, meaning it zeroes itself every half hour (Section 3.3).

For the tracer gas results, the “Low” sensor (Fig. 3, L) has the greatest ventilation rate (Fig. 5c, Table 4). This sensor position experiences flow exiting from both the back opening and a small gap at the base of the cube. This suggests that infiltration may reinforce cross ventilation within the cube for this wind direction. However, the recorded average infiltration rate of the cube (0.034 m^3 s^{-1}) is ~5% of the measured ventilation rates (Fig. 5b). The East and Mid [CO_2] sensors have similar results (Fig. 5a, c) with the Low sensor being affected by the infiltration rate, leading to faster decay rates in comparison

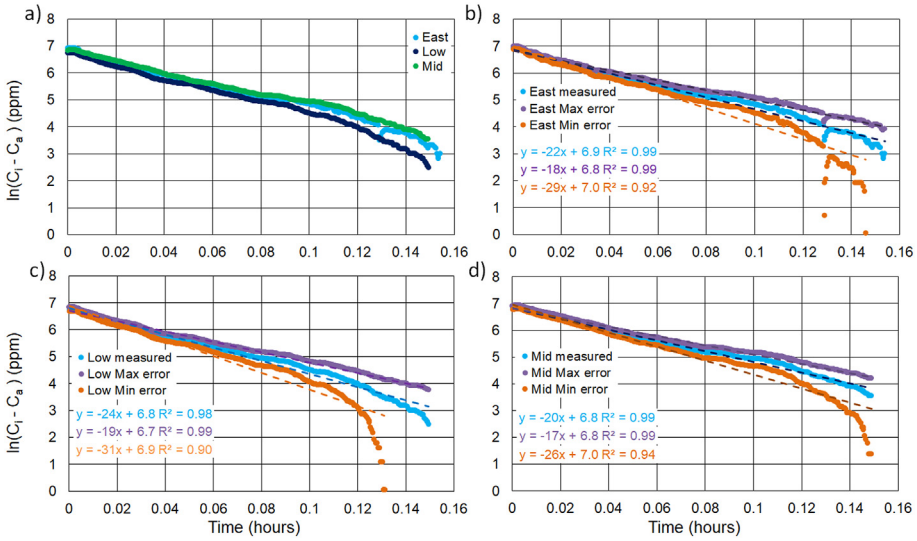

Fig. 5. Example of tracer gas decay measurements (points) with linear fits of Eqn. (3) (dashed lines) for (a) measured values from all sensors with (b–d) showing error analysis for each instrument (see Fig. 3 for positions) with equations (same colour) in the key. Max (min) error: measured value plus (minus) the maximum instrument error. (For interpretation of the references to colour in this figure legend, the reader is referred to the Web version of this article.)

(Fig. 5d). For all tracer gas releases, the error is presented as the standard deviation of the measured, maximum and minimum ventilation rates for all sensors. The infiltration rate of the cube may act against or reinforce the ventilation rate and as such is also included as an error on each ventilation rate (Table 4).

Comparison of the pressure-based normalised ventilation rate (Q_{NP}) for different averaging times (1,5, 10, and 30-min) with Q_{NT} mostly agrees within error the bounds for this case (Fig. 6). Within the release period, the pressure measurements were calibrated (gap in instantaneous results, Fig. 6).

Most of the 1-min average Q_P values are within the Q_T range. As expected, the variability of instantaneous Q_P measurements is not entirely captured by these. The 5- and 10-min averages also lie within the Q_T range. The 30-min mean Q_P is close to the lowest Q_T rate as the instantaneous Q_P values decrease after the decay period. Overall, the averaged Q_P values are closer to the lower estimate of Q_T, but shorter averaging times capture the variability of the ventilation rate. This case study suggests the pressure method tends to under-predict compared to the tracer gas method, in line with [52]. However, the missing data complicates this result. This conclusion is tested across all array, ventilation and meteorological conditions in the following sections.

4.2. Comparison of tracer gas and pressure-based ventilation rates

The normalised ventilation rates calculated from pressure (Q_{NP}) and tracer gas (Q_{NT}) data are compared for all the tracer gas release times, for both isolated and array cube cases in single-sided ventilation (Fig. 7a) and cross (Fig. 7b) configurations. There is no obvious linear relation between Q_{NP} and Q_{NT} (Table 5). However consistent with Fig. 6, both normalised ventilation rates (Fig. 7) have a similar order of magnitude. The lack of correlation between the two methods suggests that they are affected by different parameters in dissimilar ways. Straw et al. [59] used a larger (1 m^2) opening and found the pressure based method were 21% of the tracer gas ventilation rate. Across the configurations analysed, and consistent with [10] and [52]; the pressure difference method is an unreliable predictor of the ventilation rate measured through tracer gas decay.

The poor agreement for individual periods for the single-sided ventilation cases (Fig. 7a) may be caused by bi-directional flow across the opening. This process is not captured by the pressure measurements surrounding the opening. For the cross-ventilation array case (Fig. 7b), there may be improved internal mixing due to the enhanced unsteadiness of the flow with the array enhancing the effectiveness of the tracer gas measurement. However, the assumptions required for the orifice equation may not hold for cross ventilation. Some of the error for the pressure-based method may arise from the discharge coefficient used not being valid for all wind directions [29].

It must also be acknowledged that the tracer gas derived ventilation rate may not be representative of the entire cube and rather a local ventilation measurement (e.g. large errors Table 5), causing differences

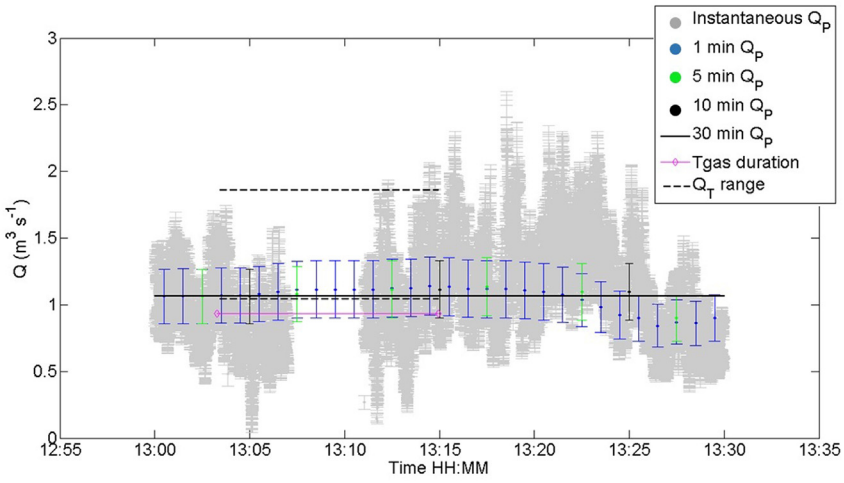

Fig. 6. Normalised tracer gas (Q_T) and pressure-based (Q_P) ventilation rates for the 21/05/2015 case study. Q_P averages for 1,5,10 and 30 min periods (black line) and for the 9 min gas release (magenta). This case study had lower errors compared to the average (Fig. 7 has more examples). Dashed lines denote the range of tracer gas ventilation rates.

Table 4
Tracer gas ventilation rate (Q_T, $m^3\ s^{-1}$) for the cross ventilated isolated cube case study on 21/05/2015 with air changes per hour (λ, h^{-1}). All calculated air change rates for the measured data have a linear fit with $R^2 > 0.97$. East, Low and Mid sensor locations shown in Fig. 3. "Measured" indicates the results from the sensor readings. "Maximum" and "minimum" are derived from the errors in the curve fit (Fig. 5). The Q_T errors are the average infiltration rate for the cube which may act against or reinforce the ventilation rate.

	East		Low		Mid	
	Q_T ($m^3\ s^{-1}$)	λ (h^{-1})	Q_T ($m^3\ s^{-1}$)	λ (h^{-1})	Q_T ($m^3\ s^{-1}$)	λ (h^{-1})
Measured	1.320 ± 0.034	22.0	1.464 ± 0.034	24.4	1.212 ± 0.034	20.2
Maximum fit	1.098 ± 0.034	18.3	1.158 ± 0.034	19.3	1.044 ± 0.034	17.4
Minimum fit	1.740 ± 0.034	29.0	1.860 ± 0.034	31.0	1.566 ± 0.034	26.1

Table 5
Analysis of the relationship between Q_{NP} and Q_{NT} as shown in Fig. 7. Analysis of the relation between Q_{NP} and Q_{NT} as shown in Fig. 7. Number of cases (#), Correlation Coefficient (R), the linear fit, R^2, P-value and errors on the measurements are listed. None of the relations are considered statistically significant.

Setup		#	R	Linear fit Q_{NP} =	R^2	P-Value	Error Q_T (%)	Error Q_p (%)	Fig
Isolated	Single sided	17	−0.02	$0.47–0.026Q_{NT}$	0.00	0.95	6–65	5–20	Fig. 7a
Isolated	Cross ventilated	23	0.01	$0.46Q_{NT}+0.4$	0.06	0.27	1–37	5–20	Fig. 7b
Array	Single sided	8	0.09	$0.26Q_{NT}+0.3$	0.00	0.84	8.3–300	5–20	Fig. 7a
Array	Cross ventilated	12	0.42	$0.24Q_{NT}+0.3$	0.17	0.17	2.8–40.3	5–20	Fig. 7b

between the two methods. The representatively of the tracer gas ventilation rate for each experiment is difficult to quantify and the cube itself may not remain well-mixed throughout the decay, as evident in deviations from the exponential decay (Fig. 5).

4.3. Effect of wind direction

When the data from Fig. 7 are analysed as a ratio (Q_{NT}/Q_{NP}) with the reference wind direction (θ_{ref}) it is evident that wind direction has an influence (Fig. 8). Large errors occur in the ratios as these are now combined across the two methods. For the single-sided case, the ratio is generally below 1, suggesting that the pressure-based method overestimates ventilation rate. For the isolated single sided cube, Q_{NT}/Q_{NP} is around 1 for $\theta_{ref} = -100°$ to $-145°$ and $\theta_{ref} = 150°$, suggesting that better agreement occurs between the methods when the flow is not impacting on the front face of the cube (opening side). For the isolated single-sided cube, as θ_{ref} decreases from 150° towards 0°, Q_{NT}/Q_{NP} tends towards 0.5, although for $\theta_{ref} = 60°–70°$ a range of Q_{NT}/Q_{NP} of 0.4–0.7 is measured.

Other factors, such as wind speed fluctuations in separated flow around the opening (causing mixing at the opening) may have an effect alongside wind direction. It also might suggest that the thermal component of the ventilation tends to act against the wind driven component for flows perpendicular to the opening, leading to a lower ventilation rate measured by the tracer gas. For the present study, internal-external temperature differences were mostly less than 5 °C, meaning that the stack effect is small and is very rarely dominant for both singled sided and cross ventilated configurations. It is unknown how representative the internal-external temperature difference is compared to the across opening difference. For both the single-sided and cross-ventilated isolated cubes there are a few points with ratios > 2, i.e. $Q_{NP} \ll Q_{NT}$. For the single-sided case this occurs when the wind is impacting the cube back and is twice the ratio of measurements for similar wind directions (Fig. 8a). For the cross ventilated cube, there are insufficient data to determine the cause (Fig. 8b).

The cross ventilated isolated cube in general has higher values of Q_{NT}/Q_{NP} than those measured for the single sided case. For the cross ventilated isolated cube, when θ_{ref} was perpendicular to the front opening ($\theta_{ref} = 0°$), Q_{NT}/Q_{NP} was approximately 0.6, increasing to 1 to 1.5 when $\theta_{ref} \sim 45°$, suggesting that it is important to note wind direction when concluding whether the pressure difference method overestimates ($Q_{NT}/Q_{NP} = 0.6$) or underestimates ($Q_{NT}/Q_{NP} = 1.5$) the ventilation rate.

This may be influenced by the internal mixing state of the cube. CFD simulations of the cube's internal flow [32,33]: a jet was present for $-45° < \theta_{ref} < 45°$ for the isolated cube; and for the array case internal flow was too unsteady for a jet to be sustained. For similar wind directions (e.g. $\theta_{ref} = 0°$) the jet was also seen via smoke visualisation for

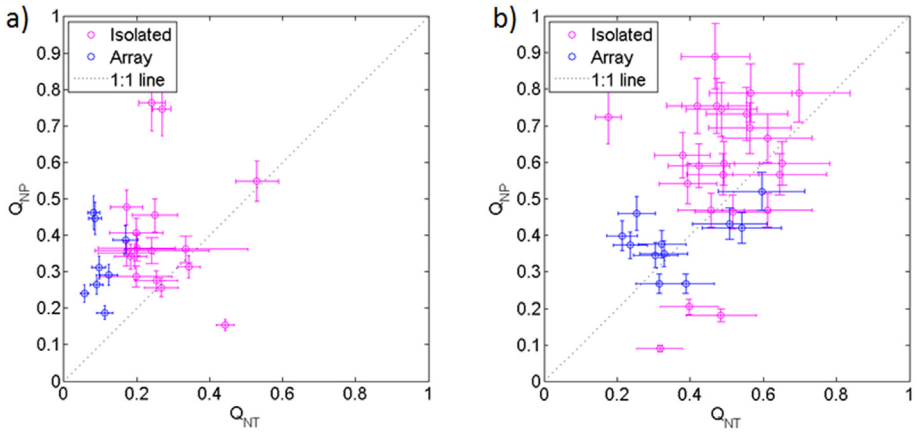

Fig. 7. Comparison of the normalised ventilation rates for pressure method (Q_{NP}) and tracer gas decay (Q_{NT}) for a) single-sided and b) cross-ventilated cases. Pressure data are averaged for the period of each tracer gas experiment. Error bars are the measurement error of the instruments propagated through equation (5) for the pressure difference method, and the standard deviation of the measured, maximum and minimum rates for the tracer gas decay (Table 4).

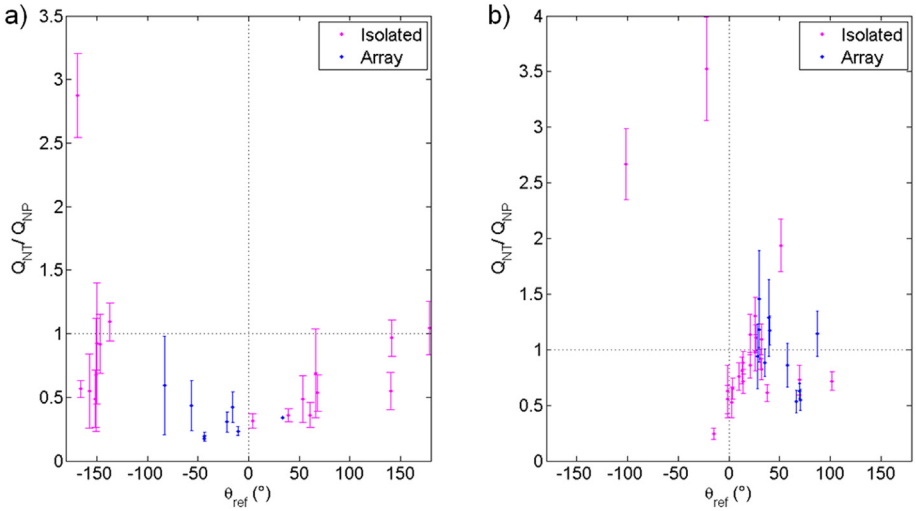

Fig. 8. Ratio of normalised ventilation rates for the two methods with reference wind direction for (a) single-sided and (b) cross ventilated cases for the array and the isolated cube.

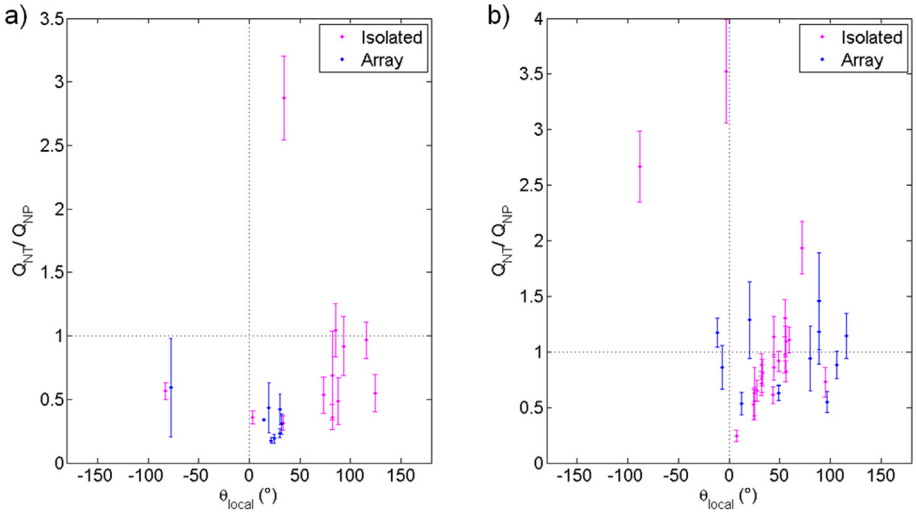

Fig. 9. As Fig. 8 but for the local wind direction (θ_{local}).

both single sided and cross ventilated cases but was often disrupted by fluctuations in wind direction. There may be better agreement between the ventilation methods when there is not a strong internal jet, and instead unsteady mixing dominates, though more data are required to confirm this. Another possible reason is the variation of C_d with wind direction, which is given one of two values in this study.

For the isolated case, θ_{ref} is similar to θ_{local} (Fig. 1) and little difference in relation with wind direction can be seen when Figs. 8 and 9 are compared. Except when the reference flow is coming from behind the cube ($\theta_{ref} = 180^{\circ}$) and θ_{local} is 45°–135° and -45° to -135°, indicating that the local mast is in the recirculation region in front of the cube. This is related to the non-linear relation between θ_{ref} and θ_{local} (for detail see [17]). Fig. 9a shows that the wide range of θ_{ref} for the single sided array corresponds to a narrow range in $\theta_{local} = 0^{\circ}$–$45^{\circ}$, suggesting that the array "channels" the flow for these reference wind directions. Q_{NT}/Q_{NP} is approximately 0.3, suggesting for when flow is not quite perpendicular to the opening, the pressure difference method consistently overestimates the ventilation rate. For the cross ventilated array case there is a wider range of θ_{local} than θ_{ref}, suggesting that the local mast is located within overlapping wakes from neighbouring cubes, and the wide spread in Q_{NT}/Q_{NP} is visible across the range in θ_{local}. Some of this spread, such as for $\theta_{local} = 90^{\circ}$, could be associated with the flow across the opening being caused by turbulent effects. Fig. 9b indicates that local wind direction alone is not enough to explain the difference in the two methods. Determining which parameters have the largest effect on the ratio between the two methods is difficult, although it is shown to be dependent on wind direction for all cases.

5. Conclusions

The large data set measured during the REFRESH Cube Campaign has enabled a detailed evaluation of two ventilation rate measurement methods (tracer gas decay, pressure-based) for a simplified building across a wide range of conditions: wind speed and direction, single-sided and cross-ventilated configurations, and isolated and staggered building array. This provides a substantial contribution to the understanding of the relative performance of the two methods under realistic meteorological conditions for a simplified built environment.

Errors in the tracer gas measurements are carefully considered. Results demonstrated that a single sensor does not necessarily give a ventilation rate representative of the whole space, and that some wind conditions led to more spatial variability and thus higher errors. Maximum and minimum fits of a decay curve to concentration data within margins of measurement error are used to estimate the error for

the ventilation rate at each measurement location; then all estimates are averaged across all three sensors.

Assessment of pressure method averaging times, suggests 10 min or greater is needed to obtain a reliable measure of the average ventilation rate within the cube. Shorter periods are too variable compared to tracer gas results. However, shorter timescales show the variability with external conditions. Agreement between the two normalised ventilation rates (tracer gas (Q_{NT}) and pressure methods (Q_{NP})) for the four configurations (single-sided and cross ventilated, isolated and array) is poor. The pressure difference method does not capture similar ventilation rates to the tracer gas methodology.

Both ventilation rate methods have their shortcomings: tracer gas - requiring a well-mixed internal environment and minimal infiltration; and pressure difference - needing knowledge of C_d and how it changes with wind direction alongside several assumptions which are unlikely to always hold in realistic outdoor flow.

The ratio Q_{NT}/Q_{NP} changes with reference wind direction. For single-sided ventilation it approached 1 when the opening was on the leeward side of the cube in the wake, and otherwise was small for windward flows, suggesting that the pressure method was an overestimate. For cross ventilation, the ratio was closer to 1 although there was more scatter. There was a slight trend for the ratio to approach 1 when the flow was not directly perpendicular to the front face for the isolated case. There may be better agreement when the internal mixing state is less dominated by a single jet, i.e. for oblique wind directions for the isolated case, and in general for the array case where external flows are highly unsteady. Sheltering may also reduce the flushing rate of the tracer gas from the cube relative to internal mixing rate.

The work could be extended by comparing the methods within controlled environments where the true ventilation rate is known, e.g. wind tunnel experiments. CFD modelling of the internal flow and tracer gas dispersion would aid sensor positioning and allow either stagnant or jet areas to be avoided or actively focused on. Whilst some of the differences between methods may be explained by changing wind directions, more work is required to explore simultaneous thermal effects, effects of sensor positioning and variations in the internal flow.

Declaration: All authors have approved the final version of the manuscript being submitted. This article is the authors' original work, has not received prior publication and is not under consideration for publication elsewhere. There are no known conflicts of interest.

Acknowledgements

This work was funded by the University of Reading and EPSRC REFRESH project (EP/K021893/1). Thanks to Solutions for Research and John Lally for assistance with the full-scale observations. Support from EPSRC LoHCool (EP/N009797/1) is also acknowledged. Datasets can be found at DOI: http://dx.doi.org/10.17864/1947.137.

Appendix A. Supplementary data

Supplementary data related to this article can be found at http://dx.doi.org/10.1016/j.buildenv.2018.03.055.

References

[1] D.N. Asimakopoulos, D.N. Assimakopoulos, N. Chrisomallidou, N. Klitsikas, D. Mangold, P. Michael, M. Santamouris, A. Tsangrassoulis, Energy and Climate in the Urban Built Environment, James & James, 2001, https://doi.org/http://dx.doi.org/10.4324/9781315073774.

[2] M. Bady, S. Kato, T. Takahashi, H. Huang, Experimental investigations of the indoor natural ventilation for different building configurations and incidences, Build. Environ. 46 (2011) 65–74 https://doi.org/10.1016/j.buildenv.2010.07.001.

[3] J.F. Barlow, O. Coceal, A Review of Urban Roughness Sublayer Turbulence, Met Office Research and Development, (2009).

[4] C.Y. Chao, M.P. Wan, A.K. Law, Ventilation performance measurement using constant concentration dosing strategy, Build. Environ. 39 (2004) 1277–1288 https://doi.org/10.1016/j.buildenv.2004.03.012.

[5] Y.-H. Chiu, D.W. Etheridge, External flow effects on the discharge coefficients of two types of ventilation opening, J. Wind Eng. Ind. Aerod. 95 (2007) 225–252 https://doi.org/10.1016/j.jweia.2006.06.013.

[6] Y. Choinière, H. Tanaka, J.A. Munroe, A. Suchorski-Tremblay, Prediction of wind-induced ventilation for livestock housing, J. Wind Eng. Ind. Aerod. 44 (1992) 2563–2574 https://doi.org/10.1016/0167-6105(92)90048-F.

[7] CO_2 meter, Product Specification CO_2 Engine K30 FR, [Available online] URL: (2013) http://co2meters.com/Documentation/Datasheets/DS-K30-FR.pdf.

[8] D. Cóstola, B. Blocken, J.L.M. Hensen, Overview of pressure coefficient data in building energy simulation and airflow network programs, Build. Environ. 44 (2009) 2027–2036 https://doi.org/10.1016/j.buildenv.2009.02.006.

[9] S. Cui, M. Cohen, P. Stabat, D. Marchio, CO2 tracer gas concentration decay method for measuring air change rate, Build. Environ. 84 (2015) 162–169 https://doi.org/10.1016/j.buildenv.2014.11.007.

[10] T.G.M. Demmers, V.R. Phillips, L.S. Short, L.R. Burgess, R.P. Hoxey, C.M. Wathes, Validation of ventilation rate measurement methods and the ammonia emission from naturally ventilated dairy and beef buildings in the United Kingdom, J. Agric. Eng. Res. 79 (2001) 107–116 https://doi.org/10.1006/jaer.2000.0678.

[11] D. Etheridge, A perspective on fifty years of natural ventilation research, Build. Environ. 91 (2015) 51–60 https://doi.org/10.1016/j.buildenv.2015.02.033.

[12] G. Evola, V. Popov, Computational analysis of wind driven natural ventilation in buildings, Energy Build. 38 (2006) 491–501 https://doi.org/10.1016/j.enbuild.2005.08.008.

[13] C. Georgakis, M. Santamouris, Experimental investigation of air flow and temperature distribution in deep urban canyons for natural ventilation purposes, Energy Build. 38 (2006) 367–376 https://doi.org/10.1016/j.enbuild.2005.07.009.

[14] C. Ghiaus, F. Allard, M. Santamouris, Urban environment influence on natural ventilation potential, Build. Environ. 41 (2006) 395–406 https://doi.org/10.1016/j.buildenv.2005.02.003.

[15] Gill Instruments, Gill R3-50 3-Axis Ultrasonic Anemometer Datasheet, [Available online] URL: (2013) http://gillinstruments.com/data/datasheets/r3-50.pdf?iss=1.20150501.

[16] H. Gough, Effects of Meteorological Conditions on Building Natural Ventilation in Idealised Urban Settings, PhD thesis University of Reading, Department of Meteorology, 2017.

[17] H. Gough, T. Sato, C. Halios, C.S.B. Grimmond, Z. Luo, J.F. Barlow, A. Robertson, A. Hoxey, A. Quinn, Effects of variability of local winds on cross ventilation for a simplified building within a full-scale asymmetric array: overview of the Silsoe field campaign, J. Wind Eng. Ind. Aerod. 175C (2018) 408–418.

[18] C.H. Halios, C.G. Helmis, K. Deligianni, S. Vratolis, K. Eleftheriadis, Determining the ventilation and aerosol deposition rates from routine indoor-air measurements, Environ. Monit. Assess. 186 (2014) 151–163 https://doi.org/10.1007/s10661-013-3362-5.

[19] N. Heijmans, P. Wouters, IEA Technical Report: Impact of the Uncertainties on Wind Pressures on the Prediction of Thermal Comfort Performances, (2002) Brussels.

[20] Honeywell, Pressure Sensors 160pc Series, [Available online] URL: (2013) https://docs-emea.rs-online.com/webdocs/0025/0900766b80025ae3.pdf.

[21] ISO-16000-1, Part 1: General Aspects of Sampling Strategy, ISO 16000-1:2004, (2004) Indoor Air 16000, 1.

[22] ISO-16000-8, Part 8: Determination of Local Mean Ages of Air in Buildings for Characterizing Ventilation Conditions ISO 16000-8:2007, (2007) Indoor Air 16000, 1.

[23] W.A. James, C.H. Daniel, POWBAM0 mechanical power balances for multi-zone building airflow analysis, Int. J. Vent. 4 (2005) 95–112.

[24] L. Ji, H. Tan, S. Kato, Z. Bu, T. Takahashi, Wind tunnel investigation on influence of fluctuating wind direction on cross natural ventilation, Build. Environ. 46 (2011) 2490–2499 https://doi.org/10.1016/j.buildenv.2011.06.006.

[25] Y. Jiang, Q. Chen, Effect of fluctuating wind direction on cross natural ventilation in buildings from large eddy simulation, Build. Environ. 37 (2002) 379–386.

[26] Y. Jiang, Q. Chen, Study of natural ventilation in buildings by large eddy simulation, J. Wind Eng. Ind. Aerod. 89 (2001) 1155–1178 https://doi.org/10.1016/S0167-6105(01)00106-4.

[27] J.C. Kaimal, J.J. Finnigan, Atmospheric Boundary Layer Flows: Their Structure and Measurement: Their Structure and Measurement, Oxford University Press, 1993.

[28] C. Karakatsanis, M.N. Bahadori, B.J. Vickery, Evaluation of pressure coefficients and estimation of air flow rates in buildings employing wind towers, Sol. Energy 37 (1986) 363–374 https://doi.org/10.1016/0038-092X(86)90132-5.

[29] P. Karava, T. Stathopoulos, A.K. Athienitis, Wind-induced natural ventilation analysis, Sol. Energy 81 (2007) 20–30 https://doi.org/10.1016/j.solener.2006.06.013.

[30] S. Kato, Flow network model based on power balance as applied to cross-ventilation, Int. J. Vent. 2 (2004) 395–408 https://doi.org/10.1080/14733315.2004.11683681.

[31] I. Khalifa, L.G. Ernez, E. Znouda, C. Bouden, Coupling TRNSYS 17 and CONTAM: simulation of a naturally ventilated double-skin fa??ade, Adv. Build. Energy Res. 9 (2015) 293–304 https://doi.org/10.1080/17512549.2015.1050694.

[32] M.-F. King, H.L. Gough, C. Halios, J.F. Barlow, A. Robertson, R. Hoxey, C.J. Noakes, Investigating the influence of neighbouring structures on natural ventilation potential of a full-scale cubical building using time-dependent CFD, J. Wind Eng. Ind. Aerod. 169 (2017) 265–279 https://doi.org/10.1016/j.jweia.2017.07.020.

[33] M.-F. King, A. Khan, N. Delbosc, H.L. Gough, C. Halios, J.F. Barlow, C.J. Noakes, Modelling urban airflow and natural ventilation using a GPU-based lattice-Boltzmann method, Build. Environ. 125 (2017) 273–284 https://doi.org/10.1016/j.buildenv.2017.08.048.

[34] Kipp, Zonen, CNR4 Instruction Manual, [Available online] URL: (2014) http://www.kippzonen.com/Product/85/CNR4-Net-Radiometer#.Wqg4EejFJPY.

[35] T.S. Larsen, P. Heiselberg, Single-sided natural ventilation driven by wind pressure and temperature difference, Energy Build. 40 (2008) 1031–1040 https://doi.org/10.1016/j.enbuild.2006.07.012.
[36] D. Laussmann, D. Helm, Air change measurements using tracer gases, Chem. Emiss. Control. Radioact. Pollut. Indoor Air Qual (2004) 365–404 https://doi.org/10.5772/1030.
[37] G.J. Levermore, A.P. Robertson, N.M. Rideout, A.D. Shea, Measurements of the performance of a wind-driven ventilation terminal, Struct. Build. 163 (2010) 129–136 https://doi.org/10.1680/stbu.2010.163.2.129.
[38] L.I.-C.O.R. Biosciences, LI-7500A Open Path CO_2 H_2O Gas Analyzer Brochure, [Available online] URL: (2009) https://www.licor.com/env/pdf/gas_analyzers/7500A/LI-7500A_brochure.pdf.
[39] H. Li, X. Li, M. Qi, Field testing of natural ventilation in college student dormitories (Beijing, China), Build. Environ. 78 (2014) 36–43 https://doi.org/10.1016/j.buildenv.2014.04.009.
[40] N. Mahyuddin, H. Awbi, A review of CO2 measurement procedures in ventilation research, Int. J. Vent. 10 (2012) 353–370 https://doi.org/10.1080/14733315.2012.11683961.
[41] N. Mahyuddin, H. Awbi, The spatial distribution of carbon dioxide in an environmental test chamber, Build. Environ. 45 (2010) 1993–2001 https://doi.org/10.1016/j.buildenv.2010.02.001.
[42] N.M. Mateus, G.N. Simões, C. Lúcio, G.C. da Graça, Comparison of measured and simulated performance of natural displacement ventilation systems for classrooms, Energy Build. 133 (2016) 185–196 https://doi.org/10.1016/j.enbuild.2016.09.057.
[43] S. Murakami, Wind tunnel test on velocity pressure field of cross-ventilation with open windows, ASHRAE Trans. 97 (1991) 525–538.
[44] N. Nikolopoulos, A. Nikolopoulos, T.S. Larsen, K.S.P. Nikas, Experimental and numerical investigation of the tracer gas methodology in the case of a naturally cross-ventilated building, Build. Environ. 56 (2012) 379–388 https://doi.org/10.1016/j.buildenv.2012.04.006.
[45] P.D. O'Sullivan, M. Kolokotroni, A field study of wind dominant single sided ventilation through a narrow slotted architectural louvre system, Energy Build. 138 (2017) 733–747 https://doi.org/10.1016/J.ENBUILD.2016.11.025.
[46] N.W.M. Ogink, J. Mosquera, S. Calvet, G. Zhang, Methods for measuring gas emissions from naturally ventilated livestock buildings: developments over the last decade and perspectives for improvement, Biosyst. Eng. 116 (2013) 297–308 https://doi.org/10.1016/j.biosystemseng.2012.10.005.
[47] E.L. Olsen, Q. Chen, Energy consumption and comfort analysis for different low-energy cooling systems in a mild climate, Energy Build. 35 (2003) 561–571 https://doi.org/10.1016/S0378-7788(02)00164-0.
[48] A. Persily, H. Levin, Ventilation measurements in IAQ studies: problems and opportunities, Proceedings of Indoor Air 2011, 12th International Conference on Indoor Air Quality and Climate, 2011.
[49] P.J. Richards, R.P. Hoxey, Pressures on a cubic building—Part 1: full-scale results, J. Wind Eng. Ind. Aerod. 102 (2012) 72–86 https://doi.org/10.1016/j.jweia.2011.11.004.
[50] A. Robertson, I. Highton, R. Hedges, Translating ventilation research into meaningful design, Proceedings of the 11th UK Conference on Wind Engineering, 2004.
[51] RS components, IEC PTFE Exposed Welded Tip Thermocouples with Miniature Thermocouple Plug-datasheet, [Available online] URL: (2013) https://docs-emea.rs-online.com/webdocs/15bb/0900766b815bb509.pdf.
[52] M. Samer, W. Berg, H.-J. Muller, M. Fiedler, M. Glaser, C. Ammon, P. Sanftleben, R. Brunsch, Radioactive 85Kr and CO 2 balance for ventilation rate measurements and gaseous emissions quantification through naturally ventilated barns, Trans. ASABE (Am. Soc. Agric. Biol. Eng.) 54 (2011) 1137–1148 https://doi.org/10.13031/2013.37105.
[53] M. Sandberg, An alternative view on the theory of cross-ventilation, Int. J. Vent. 2 (2004) 409–418.
[54] T. Schulze, U. Eicker, Controlled natural ventilation for energy efficient buildings, Energy Build. 56 (2013) 221–232 https://doi.org/10.1016/j.enbuild.2012.07.044.
[55] M.H. Sherman, Tracer-gas techniques for measuring ventilation in a single zone, Build. Environ. 25 (1990) 365–374 https://doi.org/10.1016/0360-1323(90)90010-O.
[56] H. Shetabivash, Investigation of opening position and shape on the natural cross ventilation, Energy Build. 93 (2015) 1–15 https://doi.org/10.1016/j.enbuild.2014.12.053.
[57] H.G.J. Snell, F. Seipelt, H.F.A.V. den Weghe, Ventilation rates and gaseous emissions from naturally ventilated dairy houses, Biosyst. Eng. 86 (2003) 67–73 https://doi.org/10.1016/S1537-5110(03)00113-2.
[58] G.M. Stavrakakis, M.K. Koukou, M.G. Vrachopoulos, N.C. Markatos, Natural cross-ventilation in buildings: building-scale experiments, numerical simulation and thermal comfort evaluation, Energy Build. 40 (2008) 1666–1681 https://doi.org/10.1016/j.enbuild.2008.02.022.
[59] M. Straw, C. Baker, A. Robertson, Experimental measurements and computations of the wind-induced ventilation of a cubic structure, J. Wind Eng. Ind. Aerod. 88 (2000) 213–230 https://doi.org/10.1016/S0167-6105(00)00050-7.
[60] J. Sundell, H. Levin, W.W. Nazaroff, W.S. Cain, W.J. Fisk, D.T. Grimsrud, F. Gyntelberg, Y. Li, A.K. Persily, A.C. Pickering, J.M. Samet, J.D. Spengler, S.T. Taylor, C.J. Weschler, Ventilation rates and health: multidisciplinary review of the scientific literature, Indoor Air 21 (2011) 191–204 https://doi.org/10.1111/j.1600-0668.2010.00703.x.
[61] Vaisala, Vaisala Weather Transmitter WXT520 User's Guide, (2012) https://www.vaisala.com/sites/default/files/documents/M210906EN-C.pdf.
[62] S. Van Buggenhout, a Van Brecht, S. Eren Özcan, E. Vranken, W. Van Malcot, D. Berckmans, Influence of sampling positions on accuracy of tracer gas measurements in ventilated spaces, Biosyst. Eng. 104 (2009) 216–223 https://doi.org/10.1016/j.biosystemseng.2009.04.018.
[63] T. van Hooff, B. Blocken, On the effect of wind direction and urban surroundings on natural ventilation of a large semi-enclosed stadium, Comput. Fluids 39 (2010) 1146–1155 https://doi.org/10.1016/j.compfluid.2010.02.004.
[64] G. van Moeseke, E. Gratia, S. Reiter, A. De Herde, Wind pressure distribution influence on natural ventilation for different incidences and environment densities, Energy Build. 37 (2005) 878–889 https://doi.org/10.1016/j.enbuild.2004.11.009.
[65] J. Wang, S. Wang, T. Zhang, F. Battaglia, Assessment of single-sided natural ventilation driven by buoyancy forces through variable window configurations, Energy Build. 139 (2017) 762–779 https://doi.org/10.1016/j.enbuild.2017.01.070.
[66] P.R. Warren, L.M. Parkins, Single-sided ventilation through open windows, Conf. Proc. Thermal Performance of the Exterior Envelopes of Buildings, ASHRAE, Florida, 1985p. 20.
[67] T. Yang, N. Wright, D. Etheridge, A. Quinn, A comparison of CFD and full-scale measurements for analysis of natural ventilation, Int. J. Vent. 4 (2006) 337–348.
[68] W. Yang, K. Lee, M. Chung, Characterization of indoor air quality using multiple measurements of nitrogen dioxide, Indoor Air 14 (2004) 105–111 https://doi.org/10.1046/j.1600-0668.2003.00216.x.
[69] Z. Zeng, X. Li, C. Li, Y. Zhu, Modeling ventilation in naturally ventilated double-skin fa??ade with a Venetian blind, Build. Environ. 57 (2012) 1–6 https://doi.org/10.1016/j.buildenv.2012.04.007.
[70] W. Zhang, L. Wang, Z. Ji, L. Ma, Y. Hui, Test on ventilation rates of dormitories and offices in university by the CO2 tracer gas method, Procedia Eng 121 (2015) 662–666 https://doi.org/10.1016/j.proeng.2015.08.1061.